Supporting Information (SI)

Efficient visible-light-driven Suzuki-coupling reaction over Co-doped BiOCl/Ce-doped $Bi_2O_2CO_3$ composite

Danxia Zhao[a], Guo-ping Lu[a] and Chun Cai * [a]

[a] *Chemical Engineering College, Nanjing University of Science & Technology, 200 Xiaolingwei, Nanjing 210094, P. R. China**

Tel.: +86-25-84315514; Fax: +86-25-84315030 ; e-mail: c.cai@njust.edu.cn

.

Section S1: Experimental, Characterization, Computational methodologies and models.

Scheme S1. Schematic of the Ce-doped $Bi_2O_2CO_3$ and Co-doped BiOCl/Ce-doped $Bi_2O_2CO_3$ (CBCB) composite synthesis.

Fig. S1 TEM and HRTEM images of BB.

Fig.S2 XPS spectra of the CBCB composite: (a) full spectrum, (b) Bi 4f, (c) O 1s, (d) C 1s, (e) Cl 2p, (f) Ce 3d, and (g) Co 2p.

Fig. S3 plots of $(\alpha h\nu)^2$ or $(\alpha h\nu)^{1/2}$ vs $(h\nu)$ for the band gap energy of the samples.

Fig. S4 XPS-VB spectra of the samples.

Fig. S5. EPR spectra of CBCB.

Fig. S6 XRD (a), SEM images (b) before and after the photocatalytic reaction.

Fig. S7. The TEM and HRTEM images of the recovered CBCB.

Fig. S8 (a) The band structures, and (b) total density of states and local density of states of BiOCl and C $Bi_2O_2CO_3$.

Fig. S9 Photocurrent responses of Co-doped BiOCl, Ce-doped $Bi_2O_2CO_3$ and Co-doped BiOCl/Ce-doped $Bi_2O_2CO_3$ heterojunction.

Table S1. Comparison of the catalytic activity of Co-doped BiOCl/Ce-doped $Bi_2O_2CO_3$ (CBCB) composite with conventional heterogeneous Pd catalysts in Suzuki reactions using bromobenzene and phenylboronic acid as substrates.

Table S2. Comparison of the photocatalytic activity of Co-doped BiOCl/Ce-doped $Bi_2O_2CO_3$ (CBCB) composite with previous photocatalysts in photocatalytic Suzuki reactions using bromobenzene and phenylboronic acid as substrates.

Table S3. The scope of Suzuki cross-coupling reactions with different substituents.

Table S4. ICP-MS analysis of Co or Ce in CBCB before and after the photocatalytic reaction.

Section S1.

Experimental Methods

Preparation of BiOCl and Co-doped BiOCl

In general, the synthesis of BiOCl is similar with the method in previous work [1]. 5 mmol $BiCl_3$ and 5 mmol $KMnO_4$ were each dissolved in a mixture of 20 mL of ethylene glycol and 20 mL of deionized water. Subsequently, the prepared $BiCl_3$ solution was injected into the $KMnO_4$ solution under continuous stirring. After stirring at room temperature for another 2 h, the obtained mixture was transferred into a 50 mL Teflon-lined autoclave and heated at 160 °C for 6 hours. The powders were washed with distilled water and anhydrous ethanol for three times, respectively. Then, powders were dried in vacuum at 70 ℃ for 12 h. Pure Co-doped BiOCl was prepared by the same method except that 0.6 mmol of cobaltous nitrate hexahydrate $Co(NO_3)_2 \cdot 6H_2O$ was added to the mixed solution.

Preparation of $Bi_2O_2CO_3$ and Ce-doped $Bi_2O_2CO_3$

The $Bi_2O_2CO_3$ precursor was synthesized by a hydrothermal method according to previously described process [2] with some modifications. 4 mmol bismuth citrate and 335 mg of cetyltrimethylammonium bromide (CTAB) were dispersed in 40 mL deionized water, then stirred for 30 min to form a homogeneous suspension (named as solution A).; 4 mmol Na_2CO_3 were added to 30 mL deionized water (denoted as solution B). Following this, solution B was dropped into solution A with constant stirring. After another 30 min of stirring, the obtained mixture was moved to a 100 mL Teflon-lined stainless steel autoclave and heated at 160 °C for 24 h. After being cooled down to room temperature naturally, the product was collected and washed several times with deionized water and absolute ethanol, then dried at 70°C for 12 h. Ce-doped $Bi_2O_2CO_3$ was prepared by the same method except that 0.6 mmol of Cerium nitrate hexahydrate $Ce(NO_3)_3 \cdot 6H_2O$ was added to the mixed solution.

Preparation of Co-doped BiOCl/Ce-doped $Bi_2O_2CO_3$

In a typical procedure, 200 mg Ce-$Bi_2O_2CO_3$ and 5 mmol $KMnO_4$ were each dissolved in 20 ml of de-ionized water, and the former was ultrasonically dispersed for 30 min to form a homogeneous suspension (denoted as solution A). 5 mmol $BiCl_3$ and 0.6 mmol $Co(NO_3)_2 \cdot 6H_2O$ were dissolved in 30 ml ethylene glycol to form a homogeneous solution B. Subsequently, the prepared A and B solutions were added dropwise to the $KMnO_4$ solution under continuous stirring. After 2 h, the obtained mixture was moved to a 100 mL Teflon-lined stainless steel autoclave and heated at 160 °C for 6 h and a brown powder product was obtained. Finally, the powder (named as CBBC) was centrifuged and washed with de-ionized water and ethanol several times before being dried at 70 °C for 12 h. For comparison, the $BiOCl/Bi_2O_2CO_3$ composite was prepared according to the same procedure except for the precursor without cobalt and cerium ions, and marked as BB.

Characterization of photocatalysts

X-ray diffractometry (XRD) using a Shimadzu XRD-6000 diffractometer with Cu Kα irradiation. Scanning electron microscopy (SEM) images was performed using a Hitachi S-4800. TEM images were taken using a PHILIPS Tecnai 12 microscope operating at 120 kv. Energy Dispersive X-ray Spectroscopic analysis (EDS) was performed with a JEM-2010(HR) transmission electron microscope at an acceleration voltage of 200kV. High Resolution Transmission electron microscopy (HRTEM) was performed on Philips-FEI Tecnai G2 F20 operating at 300kv. Nitrogen adsorption-desorption analysis was conducted using a Micromeritics ASAP 2020 at 77 K. In addition, X-ray photoelectron spectroscopy (XPS) was performed on an ESCALAB 250Xi spectrometer, using an Al Kα X-ray source (1486.6 eV of photons), which was calibrated by setting the C 1s peak to 284.80 eV. Inductively coupled plasma mass spectrometer (ICP-MS) was analyzed on Optima 7300DV. The UV - Vis diffuse reflectance spectra of the catalysts were recorded on a UV - Vis spectrometer (Lambda 750) within the range of 200 - 1100 nm. Photoluminescence spectra (PL) of the catalysts were carried out on a spectrophotometer (LabRAM HR Evolution).

Electrochemical measurements

Electrochemical and photoelectrochemical measurements were carried out on an electrochemical workstation (CHI 660E, Shanghai) with a standard three-electrode system. The powder coated on indium-tin-oxide (ITO) glass substrate was applied as the working electrode. 10 mg powder was suspended into 1 mL absolute ethanol and then the slurry was dropwise added on a ITO substrate (15mm × 30 mm). The working electrode was exposed to air for 10 h to remove the ethanol. Platinum wire and Ag/AgCl electrode were used as the counter electrode and reference electrode, respectively. The electrolyte was 0.1 M Na_2SO_4 solution and illumination source was a 300 W Xe lamp providing simulated solar light.

EPR experiment

The h^+ radical signals in solution in the dark were determined using electron spin resonance (EPR; JES FA200).

Computational methodologies and models

First-principle calculations within the framework of density functional theory (DFT) were performed by employing the program Vienna *ab initio* simulation package (VASP) [3]. The valence electronic states are described using periodic plane wave and the electron-ion interactions are described by the projector augmented wave (PAW) approach [4]. The exchange and correlation potential is treated by the generalized gradient approximation (GGA) in the Perdew-Burke-Ernzerhof (PBE) form [5]. The valence electron configurations included in the calculations are Bi ($6s^26p^3$), Cl ($3s^23p^5$), O ($2s^22p^4$), C ($2s^22p^2$), Co ($3d^84s^1$),

and Ce ($4f^15s^25p^65d^16s^2$). The cutoff energy of plane-wave basis is set to be 400 eV. The lattice constants and atomic positions were both fully relaxed until electronic self-consistent and Hellmann-Feynman forces on atoms converge were reached at 10^{-6} eV and 0.005eV/Å, respectively. The Brillouin zone was sampled by the Monkhorst-Pack [6] k-point grid with densities of 0.2 $Å^{-1}$.

To construct the aspired interface structures, the (001) surfaces of both BiOCl and $Bi_2O_2CO_3$ were employed to decrease the misfit. By cleaving fully relaxed bulk materials perpendicular to *c*-axis, the exposed (001) facets of BiOCl and $Bi_2O_2CO_3$ surfaces are constructed. The BiOCl/$Bi_2O_2CO_3$ heterostructures are constructed by putting two surface slabs together. The interface model employed the average size of both BiOCl and $Bi_2O_2CO_3$ slabs to make a small mismatch (~ 1%) along the *a*- and *b*-axis.

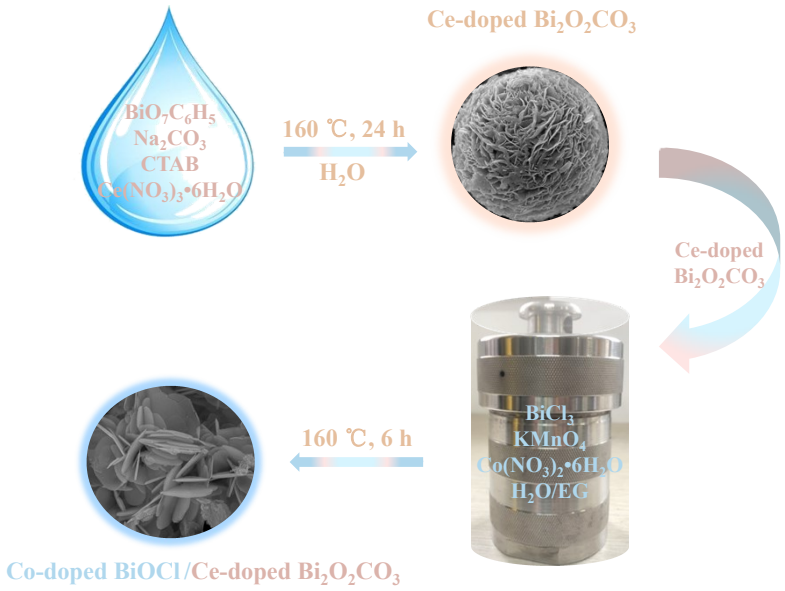

Scheme S1. Schematic of the Ce-doped $Bi_2O_2CO_3$ and Co-doped BiOCl/Ce-doped $Bi_2O_2CO_3$ (CBCB) composite synthesis.

The CO_3^{2-} groups are interleaved into the stack of $(Bi_2O_2)^{2+}$ sheets to flower-like form $Bi_2O_2CO_3$. $Bi_2O_2CO_3$ acts as the precursor to mediate the subsequent growth of BiOCl nanosheets. $Bi_2O_2CO_3$ and BiOCl have similar aurivillius structure, and the shared layers with alternative stacking $(Bi_2O_2)^{2-}$ sheets were interleaved by CO_3^{2-} or Cl^- groups for BiOCl/$Bi_2O_2CO_3$ composite. Shown as Scheme 1, the BiOCl/$Bi_2O_2CO_3$ composites retain the original flower-like shape of the $Bi_2O_2CO_3$ precursor. This means that the BiOCl nanosheets are in situ formed and have intimate contacts with the $Bi_2O_2CO_3$ nanosheets to form heterojunction, which can effectively facilitate the transfer of photogenerated charge carriers between them.

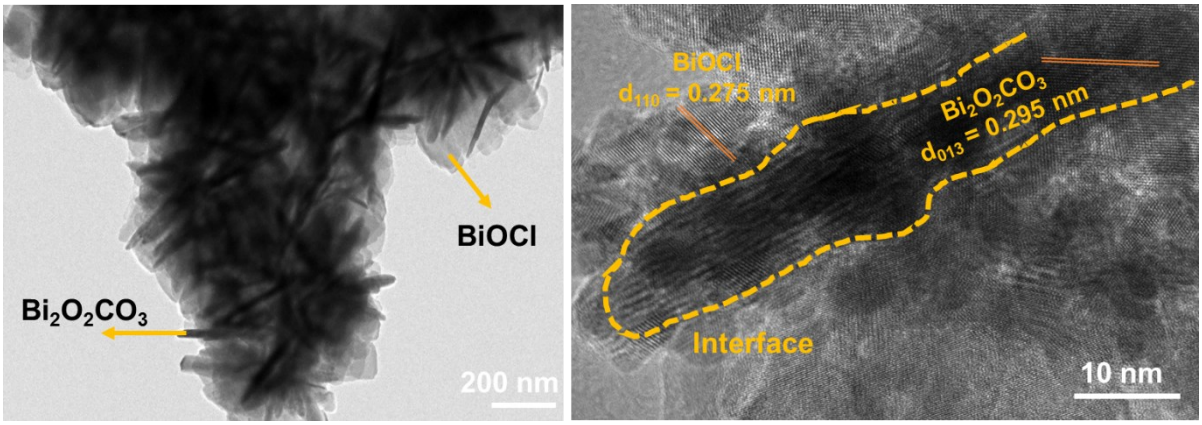

Fig. S1 TEM and HRTEM images of BB.

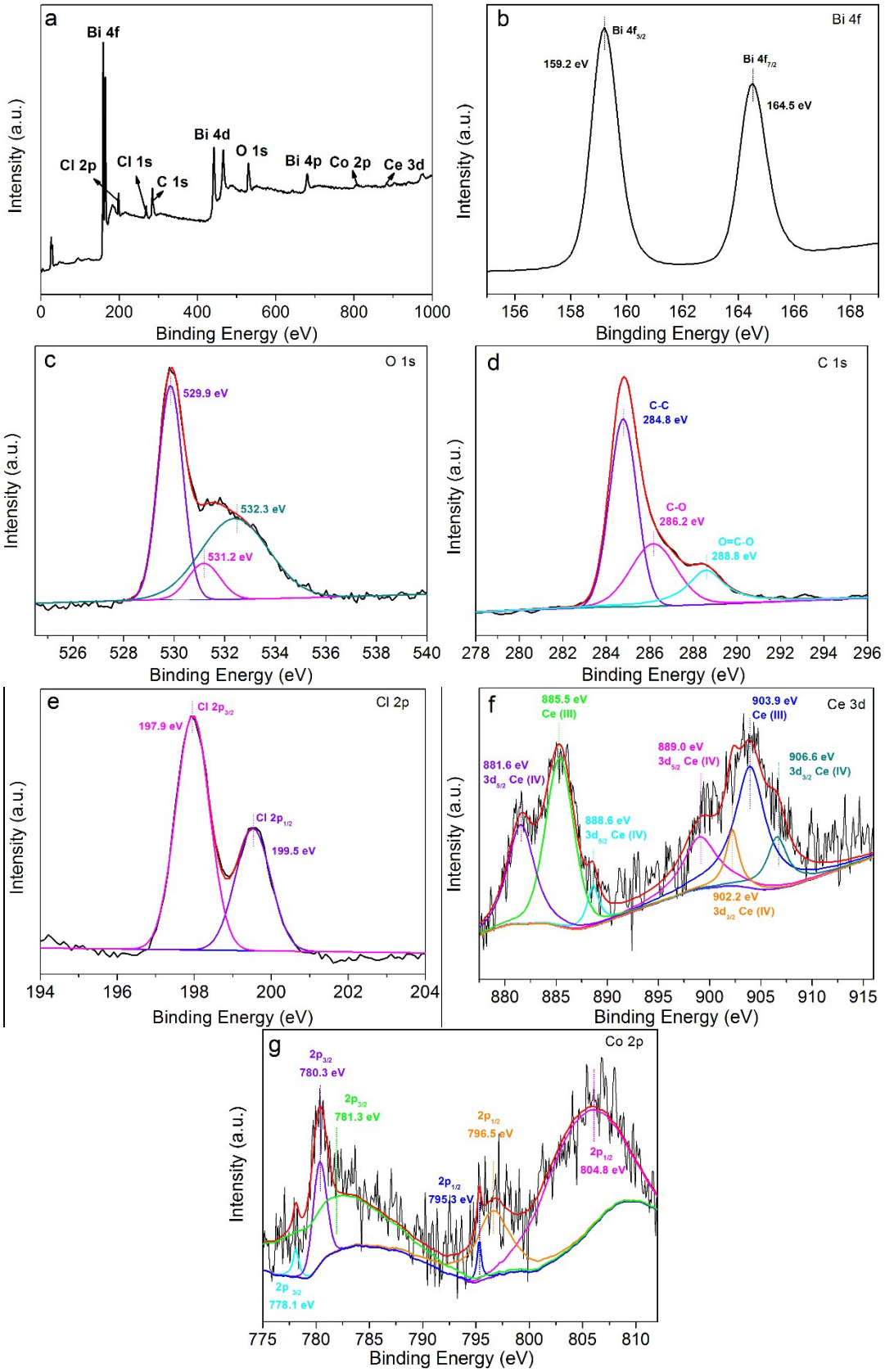

Fig. S2 XPS spectra of the CBCB composite: (a) full spectrum, (b) Bi 4f, (c) O 1s, (d) C 1s, (e) Cl 2p, (f) Ce 3d, and (g) Co 2p.

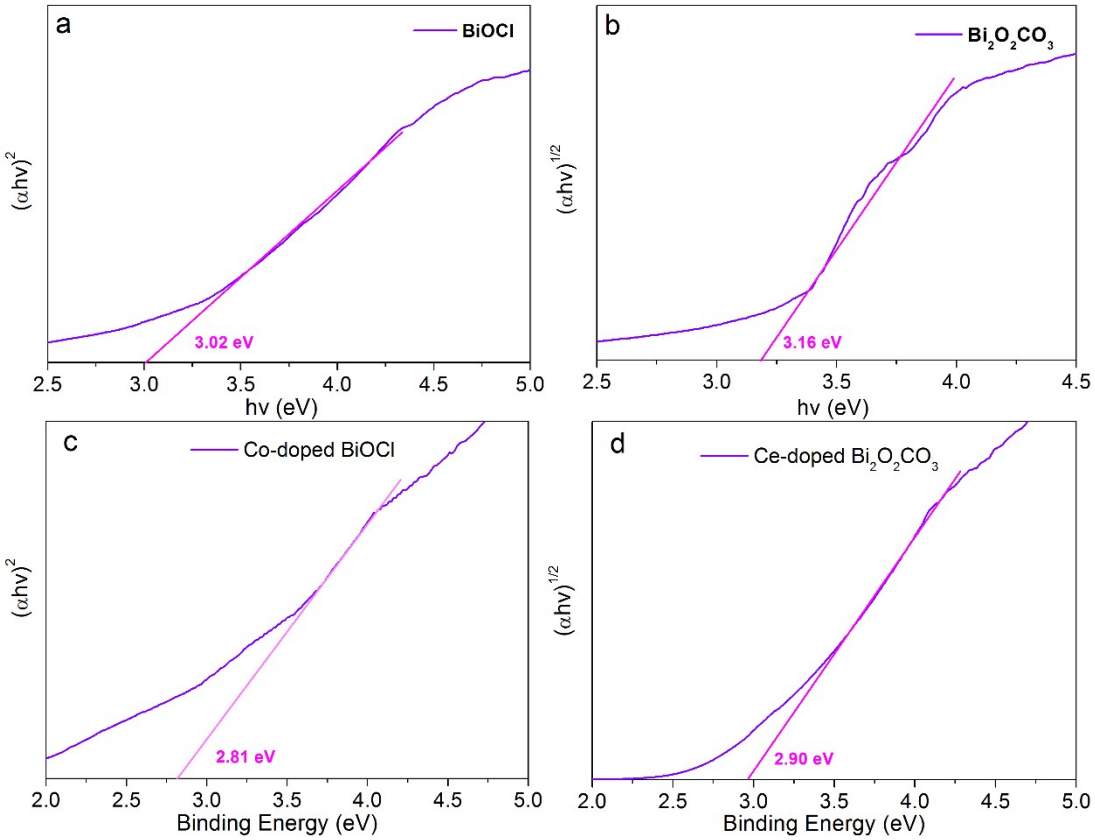

Fig. S3 plots of $(\alpha h\nu)^2$ or $(\alpha h\nu)^{1/2}$ vs $(h\nu)$ for the band gap energy of the samples.

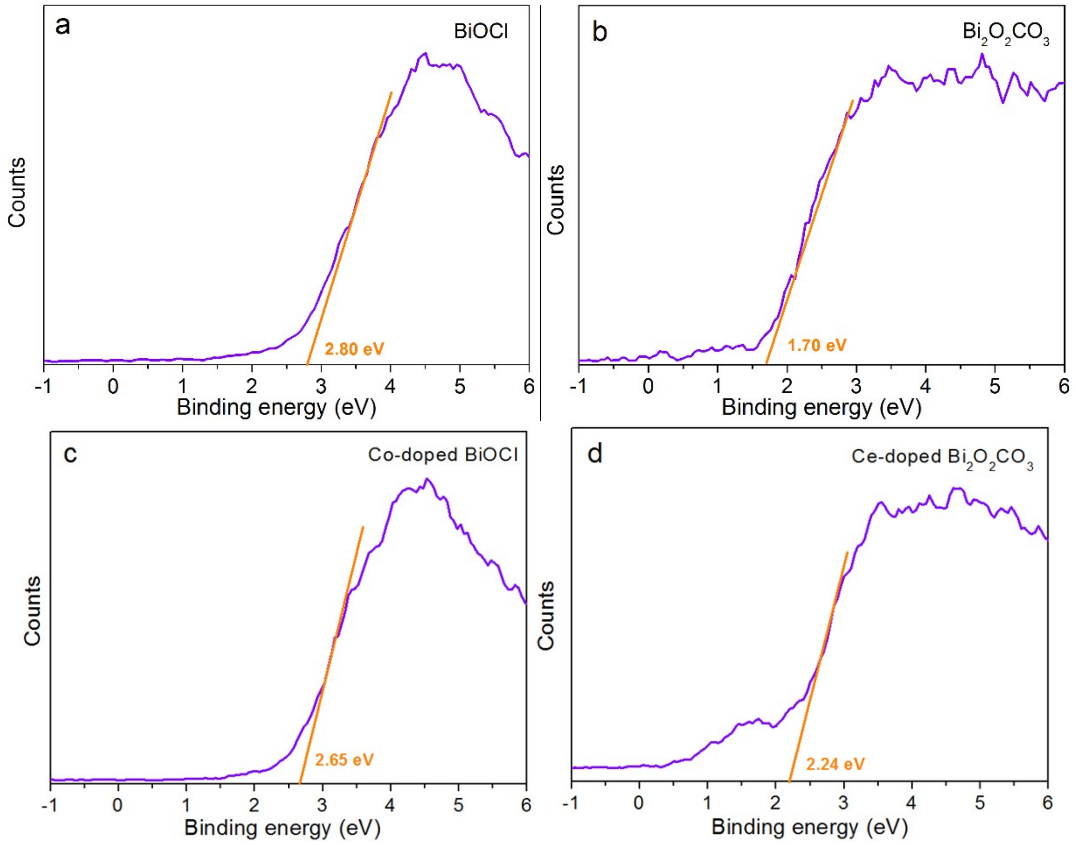

Fig. S4. XPS-VB spectra of the samples.

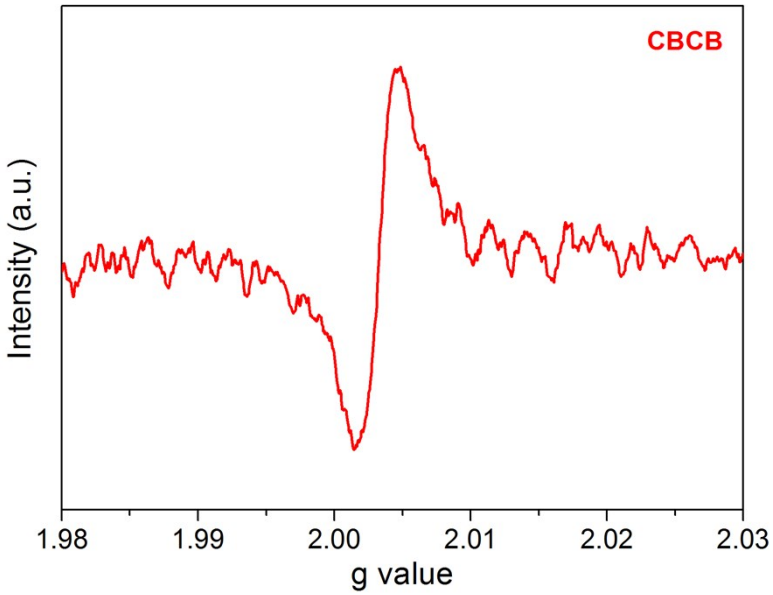

Fig. S5. EPR spectra of CBCB.

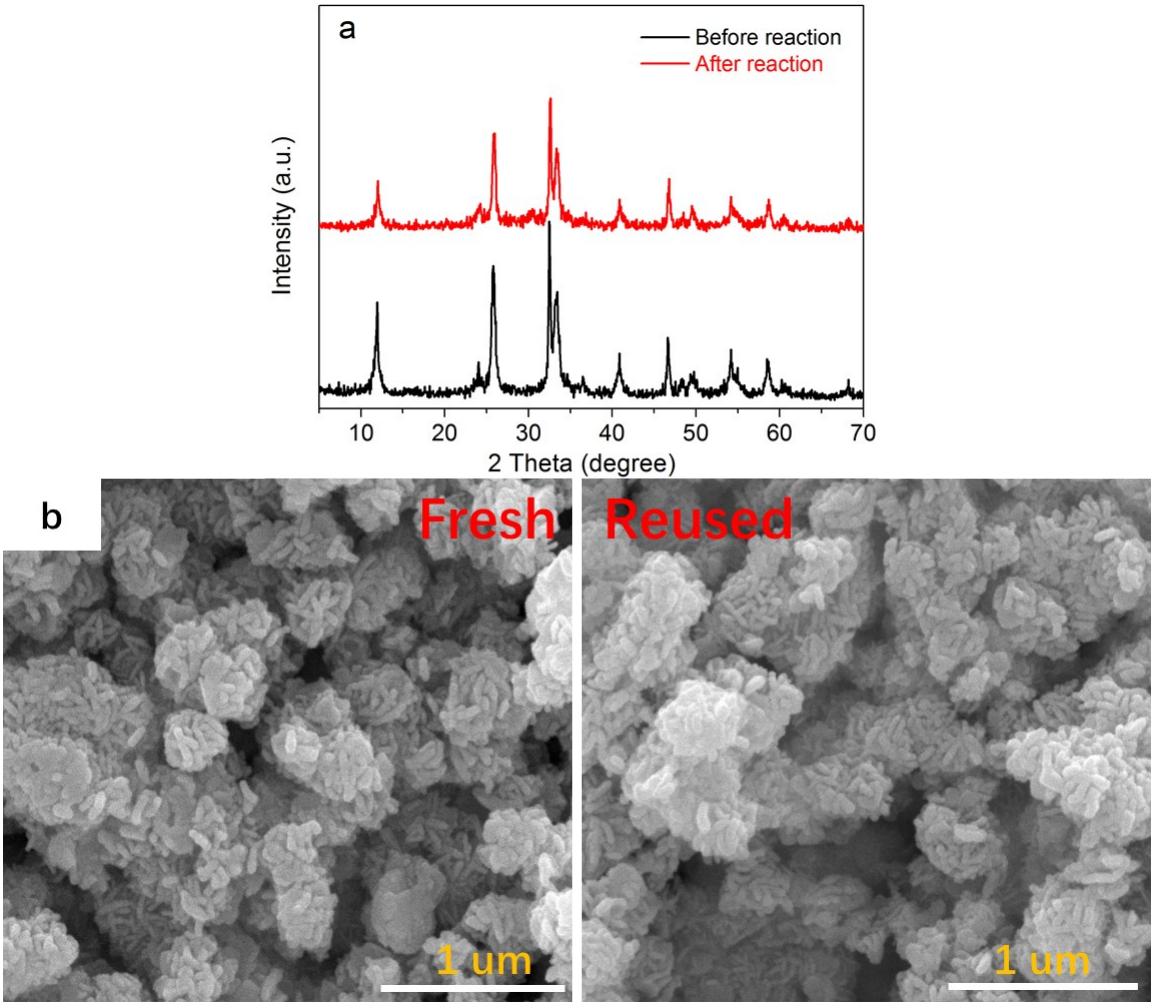

Fig. S6. XRD (a), SEM images (b) before and after the photocatalytic reaction.

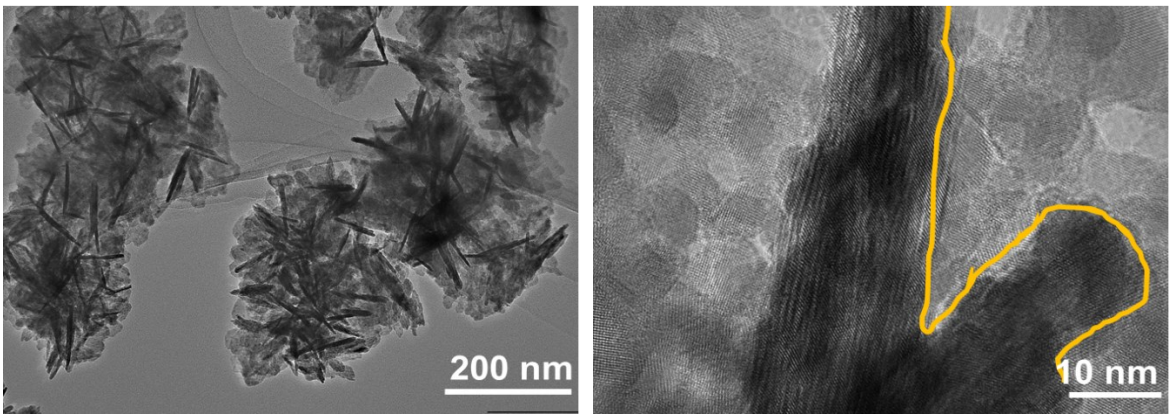

Fig. S7. The TEM and HRTEM images of the recovered CBCB.

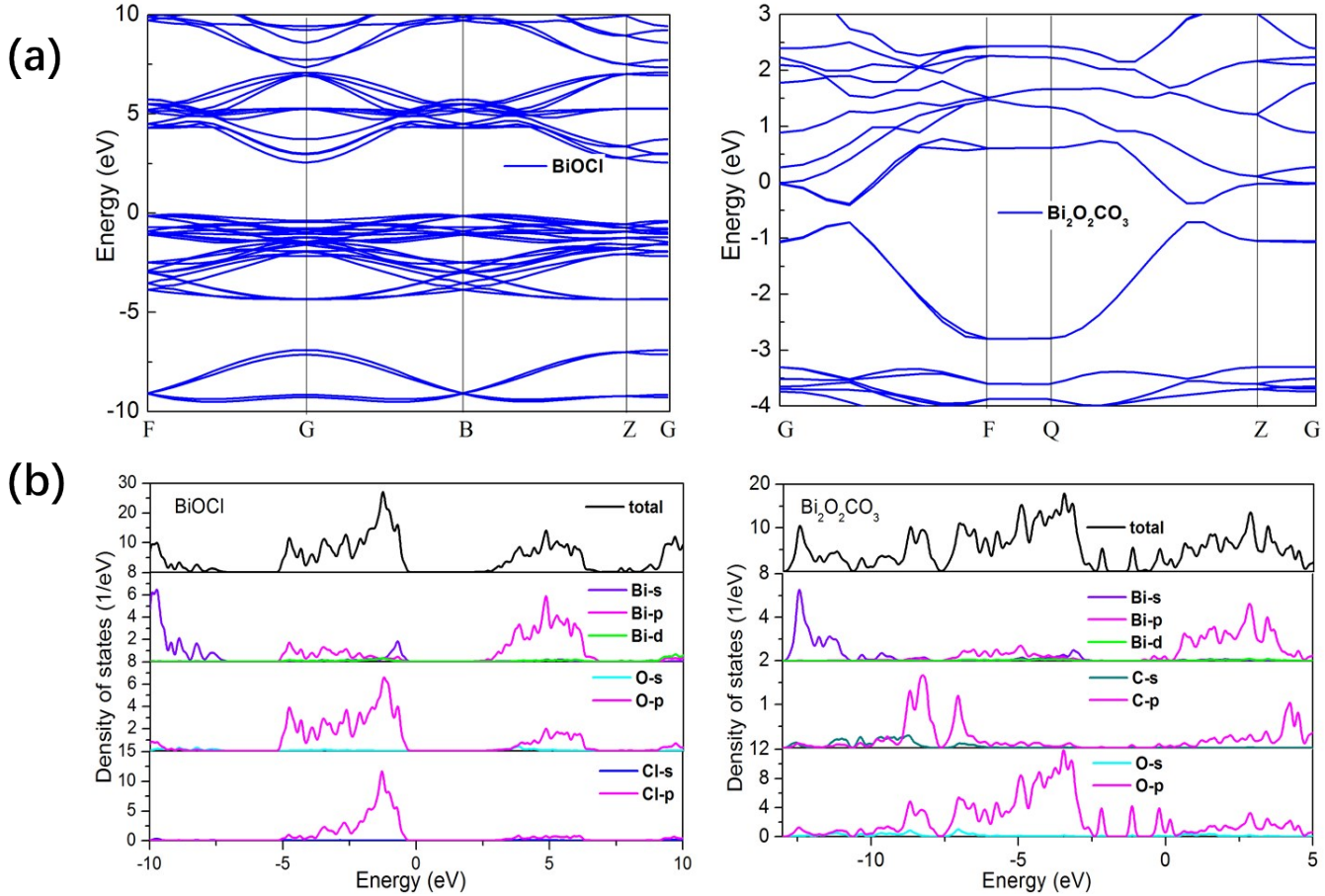

Fig. S8 (a) The band structures, and (b) total density of states and local density of states of BiOCl and C $Bi_2O_2CO_3$.

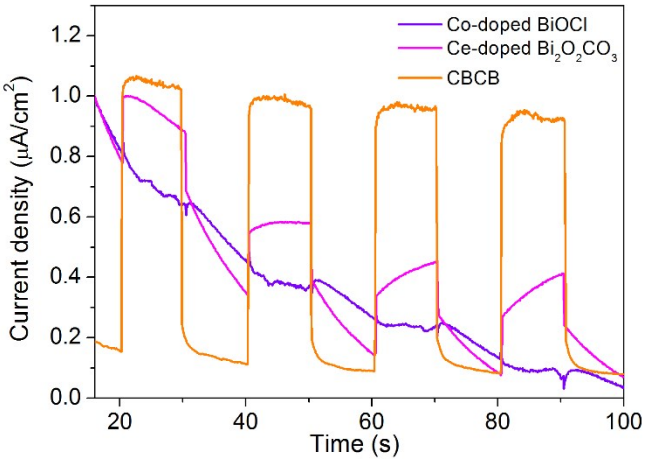

Fig. S9. The photocurrent responses of Co-doped BiOCl, Ce-doped $Bi_2O_2CO_3$ and Co-doped BiOCl/Ce-doped $Bi_2O_2CO_3$ heterojunction.

Table S1. Comparison of the catalytic activity of Co-doped BiOCl/Ce-doped $Bi_2O_2CO_3$ (CBCB) composite with conventional heterogeneous Pd catalysts in Suzuki reactions using bromobenzene and phenylboronic acid as substrates

Entry	Catalysts	Conditions	Yield [%]
1	**palladium-free CBCB in this work**	**RT, EtOH/H_2O, 16 h**	**91**
2	Pd-G-3[7]	Reflux, EtOH, 24 h	42
3	G4-OH Pd NPs[8]	153 °C, DMF,48 h	70
4	MUA-Pd[9]	90 °C, DMF,12 h	92
5	Pd-Fe_3O_4[10]	Reflux, DME/H_2O, 48 h	70
6	Pd-CNT-ED-OH[11]	120 °C, DMF,24 h	90
7	Pd@MTiO_2[12]	70°C, H_2O, 4 h	95
8	Pd-DBS-$CONHNH_2$[13]	50°C, EtOH/H_2O, 18 h	86
9	Y_3Pd_2[14]	60°C, DMF/H_2O, 8 h	98
10	PdO_x/NiO NFs[15]	35°C, EtOH/H_2O, 2 h	85
11	HEC-NHC-Pd[16]	60 °C, EtOH/H_2O, 2 h	97

Table S2. Comparison of the photocatalytic activity of Co-doped BiOCl/Ce-doped $Bi_2O_2CO_3$ (CBCB) composite with previous photocatalysts in photocatalytic Suzuki reactions using bromobenzene and phenylboronic acid as substrates

Entry	Catalysts	Conditions	Yield [%]
1	**palladium-free CBCB in this work**	**RT, EtOH/H_2O, 16 h, 15 W white LED**	**91**
2	Au-Pd alloy[17]	30 °C, EtOH/CTAB, 3 h, visible light 0.5 W cm^{-2}	80
3	Pd/Au/PN-CeO_2[18]	25 °C, DMF/H_2O, 1 h, 150 W Xe lamp	98
4	Pd-MoS_2 nanosheets[19]	EtOH/H_2O, Solar-light 12:00 PM to 14:00 PM	80
5	$NiFe_2O_4$/2D MoS_2-Pd[20]	30 °C, EtOH/H_2O, 5 h, 300 W Xe lamp	43
6	HUY@S-TOH/AuPd[21]	25 °C, EtOH/H_2O, 3 h, 300 W Xe lamp	88
7	St-MOP@Pd-2[22]	25 °C, MeOH, 5h, white LED (0.9 mW cm^{-2})	51
8	Pd@NiO_{80}/SiC[23]	30 °C, DMF/H_2O, 5 h, Xe lamp (0.35 W cm^{-2})	83
9	Pd-Azo-POP[24]	25 °C, EtOH/H_2O, 4 h, 350 W Xe lamp	99
10	Pd/$PbTiO_3$[25]	80 °C, EtOH/H_2O, 20 min, UV (300 W) + MW (600 W)	78
11	CoPc/NiO[26]	27 ± 2 °C, DMF/H_2O, 8 h, 20 W white LED	78

Table S3. The scope of Suzuki cross-coupling reactions with different substituents

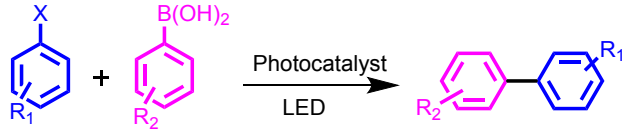

1 **2**

Entry	Reactant 1	Reactant 2	Product	Yield (%)[b]
1	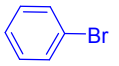	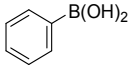	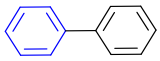	91
2	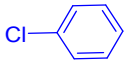	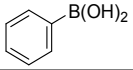	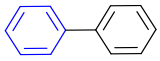	88
3	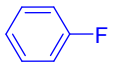	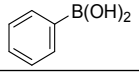	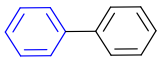	71
4	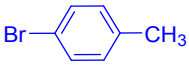	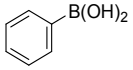	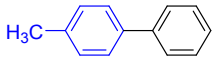	44
5	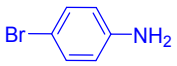	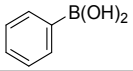	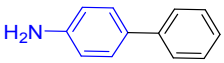	15
6	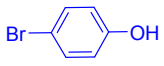	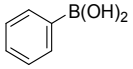	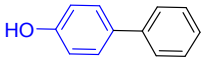	20
7	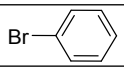	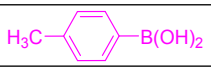		65
8	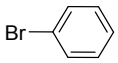	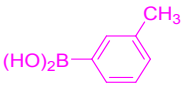	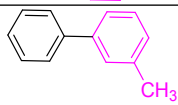	54
9	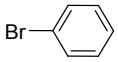	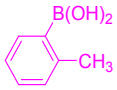	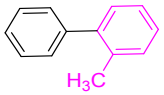	32
10	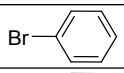	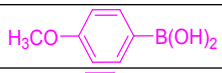	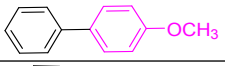	70
11	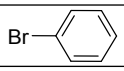	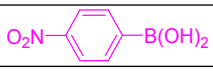	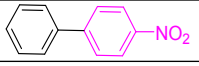	18

[a]Experiment: Halide (0.2 mmol); aryl boronic acid (0.22mmol); K_2CO_3 (0.45 mmol); CBCB (25 mg); 1:1 EtOH/H_2O,3 ml; RT; atmospheric pressure; 16 h; 15 W white LED. [b]Yields were determined by GC-MS and GC with m-xylene as the interior label.

Table S4. ICP-MS analysis of Co or Ce in CBCB before and after the photocatalytic reaction.

Material (CBCB)	Element		Metal Content (mg/kg)	
Before	Co	Ce	9823.8 (Co)	2282 (Ce)
After	Co	Ce	9612 (Co)	2137 (Ce)

References

1. S. Niu, R. Zhang and C. Guo, *Mater. Chem. Front.*, 2020, **4**, 2314-2324.
2. Y. Lan, Z. Li, W. Xie, D. Li, G. Yan, S. Guo, C. Pan and J. Wu, *J. Hazard. Mater.*, 2020, **385**, 121622.
3. G. Kresse and J. Furthmüller, *Comp. Mater. Sci.,* 1996, **6**, 15-50.
4. P. E. Blöchl, *Phys. Rev. B*, 1994, **50**, 17953-17979.
5. J. P. Perdew, K. Burke and M. Ernzerhof, *Phys. Rev. Lett.*, 1996, **77**, 3865-3868.
6. J. D. Pack and H. J. Monkhorst, *Physical Review B*, 1977, **16**, 1748-1749.
7. K. R. Gopidas, J. K. Whitesell and M. A. Fox, *Nano Letters.*, 2003, **3**, 1757-1760.
8. M. Pittelkow, K. Moth-Poulsen, U. Boas and J. B. Christensen, *Langmuir.*, 2003, **19**, 7682-7684.
9. M. Cargnello, N. L. Wieder, P. Canton, T. Montini, G. Giambastiani, A. Benedetti, R. J. Gorte and P. Fornasiero, *Chemistry of Materials*, 2011, **23**, 3961-3969.
10. Y. Jang, J. Chung, S. Kim, S. W. Jun, B. H. Kim, D. W. Lee, B. M. Kim and T. Hyeon, *Phys. Chem. Chem. Phys.*, 2011, **13**, 2512-2516.
11. E. Kim, H. S. Jeong and B. M. Kim, *Cata. Commun.*, 2014, **46**, 71-74.
12. P. Mondal, P. Bhanja, R. Khatun, A. Bhaumik, D. Das and S. Manirul Islam, *J. Colloid. Interf. Sci.*, 2017, **508**, 378-386.
13. P. Slavík, D. W. Kurka and D. K. Smith, *Chem. Sci.*, 2018, **9**, 8673-8681.
14. T.-N. Ye, Y. Lu, Z. Xiao, J. Li, T. Nakao, H. Abe, Y. Niwa, M. Kitano, T. Tada and H. Hosono, *Nature Commun.*, 2019, **10**.
15. T. Wang, X. Tao, D. Wu, X. Lu, Q. Yu, S. Liu, H. Chen and B. Li, *The J. Phys. Chem. C*, 2020, **124**, 22539-22549.
16. Y. Dong, J. Bi, S. Zhang, D. Zhu, D. Meng, S. Ming, K. Qin, Q. Liu, L. Guo and T. Li, *Appl. Surf. Sci.* 2020, **531**, 147392.
17. Q. Xiao, S. Sarina, E. Jaatinen, J. Jia, D. P. Arnold, H. Liu and H. Zhu, *Green Chem.,* 2014, **16**.
18. S. Zhang, C. Chang, Z. Huang, Y. Ma, W. Gao, J. Li and Y. Qu, *ACS Catal.*, 2015, **5**, 6481-6488.
19. H. H. Shin, E. Kang, H. Park, T. Han, C.-H. Lee and D.-K. Lim, *J. Mater. Chem. A,* 2017, **5**, 24965-24971.
20. W. Fu, X. Xu, W. Wang, J. Shen and M. Ye, *ACS Sustain. Chem. Eng.*, 2018, **6**, 8935-8944.
21. S. Rohani, A. Ziarati, G. M. Ziarani, A. Badiei and T. Burgi, *Catal. Sci. Technol.,* 2019, **9**, 3820-3827.
22. S. H. Ryu, S. J. Choi, J. H. Seon, B. Jo, S. M. Lee, H. J. Kim, Y.-J. Ko, K. C. Ko, T. K. Ahn and S. U. Son, *Catal. Sci. Technol.,* 2020, **10**, 5535-5543.
23. Z.-F. Jiao, Y.-M. Tian, B. Zhang, C.-H. Hao, Y. Qiao, Y.-X. Wang, Y. Qin, U. Radius, H. Braunschweig, T. B. Marder, X.-N. Guo and X.-Y. Guo, *J. Catal.,* 2020, **389**, 517-524.

24. J. Chakraborty, I. Nath and F. Verpoort, *Chem. Eng. J.,* 2019, **358**, 580-588.
25. J. Wen, L. Ling, Y. Chen and Z. Bian, *Chinese J. Catal.*, 2020, **41**, 1674-1681.
26. P. K. Prajapati, S. Saini and S. L. Jain, *J. Mater. Chem. A,* 2020, **8**, 5246-5254.